Journal of Chromatography A, 1218 (2011) 2912–2922

Contents lists available at ScienceDirect

Journal of Chromatography A

journal homepage: www.elsevier.com/locate/chroma

Influence of the pore size of reversed phase materials on peptide purification processes

David Gétaz [a], Nihan Dogan [a], Nicola Forrer [b], Massimo Morbidelli [a,c,*]

[a] Department of Chemistry and Applied Bioscience, Institute for Chemical and Bioengineering, ETH Zurich, CH-8093 Zurich, Switzerland
[b] Zeochem AG, CH-8707 Uetikon, Switzerland
[c] Dipartimento di Chimica, Materiali e Ingegneria Chimica "Giulio Natta", Politecnico di Milano, 20131 Milano, Italy

ARTICLE INFO

Article history:
Received 20 December 2010
Received in revised form 1 March 2011
Accepted 4 March 2011
Available online 12 March 2011

Keywords:
Pore size
Chromatography
Reversed-phase
Peptide
Surface area

ABSTRACT

The influence of the pore size of a chromatographic reversed phase material on the adsorption equilibria and diffusion of two industrially relevant peptides (i.e. a small synthetic peptide and insulin) has been studied using seven different reversed phase HPLC materials having pore sizes ranging from 90 Å to 300 Å. The stationary phase pore size distribution was obtained by inverse size exclusion measurement (iSEC). The effect of the pore size on the mass transfer properties of the materials was evaluated from Van Deemter experiments. It has been shown that the lumped mass transfer coefficient increases linearly with the average pore size. The Henry coefficient and the impurity selectivity were determined in diluted conditions. The saturation capacity of the main peptides was determined in overloaded conditions using the inverse method (i.e. peak fitting). It was shown that the adsorption equilibria of the peptides on the seven materials is well described by a surface-specific adsorption isotherm. Based on this a lumped kinetic model has been developed to model the elution profile of the two peptides in overloaded conditions and to simulate the purification of the peptide from its crude mixture. It has been found that the separation of insulin from its main impurity (i.e. desamido-insulin) was not affected by the pore size. On the other hand, in the case of the synthetic peptide, it was found that the adsorption of the most significant impurity decreases with the pore size. This decrease is probably due to an increase in silanol activity with decreasing pore size.

1. Introduction

Among the chromatographic techniques, reversed-phase high-performance liquid chromatography (RP-HPLC) is the method of choice for peptide purification. In reversed-phase chromatography, a very broad range of stationary phases is available. These can be made of different materials (e.g. silica based, polymer based, silica based with a polymer coating. . .) and they can have different pore size, particle size and functionalization. The broad range of surface chemistry available on the market is very important to allow selecting the phase providing the best selectivity for the molecule of interest. On the other hand, the pore size and the particle size are very important factor influencing the analyte diffusion in the porous particle and therefore the peak broadening process.

The effect of the pore size on the resolution in diluted conditions is relatively well understood. In general, the diffusion inside the porous particle is enhanced by increasing values of the ratio between pore size and molecule size [1]. Sands et al. have investigated the effect of the pore size on the resolution of small molecules and peptides in diluted conditions [2]. More recently, Gritti et al. have compared the efficiency of columns packed with partially and totally porous particle both in diluted [3] and overloaded conditions [4]. They have shown that the adsorption equilibria on these two different materials are very similar if the adsorption is normalized by the accessible surface area. Several authors have suggested the use of surface concentration to describe the adsorption process in chromatography [2,4–8]. The main advantage of this normalization is that it enables to compare stationary phases with different surface areas provided that they have the same surface chemistry.

In this work, the effect of the pore size on the adsorption equilibria and diffusion of two industrially relevant peptides has been studied. The stationary phases pore size distribution was obtained from iSEC measurements. The effect of the pore size on the mass transfer inside the particle has been evaluated from Van Deemter experiments. The surface-specific Henry coefficient and saturation capacity of the main peptides were determined. The results were then implemented in a lumped kinetic model including a surface-specific adsorption isotherm. This model was able to account for

* Corresponding author at: Department of Chemistry and Applied Bioscience, Institute for Chemical and Bioengineering, ETH Zurich, CH-8093 Zurich, Switzerland. Tel.: +41 632 30 34; fax: +41 632 10 82.
E-mail address: massimo.morbidelli@chem.ethz.ch (M. Morbidelli).

0021-9673/$ – see front matter © 2011 Elsevier B.V. All rights reserved.
doi:10.1016/j.chroma.2011.03.008

differences in the stationary phase pore size. It was used to predict the elution profile and the separation of the peptide from its main impurities and to compare the performances of stationary phases exhibiting different pore sizes but identical chemical composition.

2. Theory

2.1. Model of the chromatographic column

In chromatography, the lumped kinetic model is very often used to quantify processes under overloaded conditions. The mass balance of this model for a solute i is written as follow [9]:

$$\frac{\partial c_i}{\partial t} + \Phi_i \frac{\partial q_i}{\partial t} + u_{lin} \frac{\partial c_i}{\partial z} = D_{L,i} \frac{\partial^2 c_i}{\partial z^2} \quad (1)$$

where c_i and q_i are the concentrations of component i in the mobile and in the adsorbed phase respectively; z and t are the spatial and time coordinate; u_{lin} is the linear mobile phase velocity; D_L is the axial dispersion coefficient and Φ_i is the phase ratio. The mass transport between stationary and mobile phases is described using the solid film linear driving force model:

$$\frac{\partial q_i}{\partial t} = k_{M,i}(q_{eq,i} - q_i) \quad (2)$$

where $k_{M,i}$ is the lumped mass transfer coefficient and $q_{eq,i}$ is the concentration of component i adsorbed in equilibrium with the amount in the mobile phase, i.e. c_i.

In Eq. (1), the term $\Phi_i(\partial q_i/\partial t)$ represents the accumulation of component i in the adsorbed phase in terms of mass per unit time and unit liquid volume. Therefore, its units are $\mathrm{mg\,s^{-1}\,mL^{-1}}$. In chromatography, the amount of component i adsorbed q_i is typically referred to the solid volume. Its units are $\mathrm{mg\,mL^{-1}}$ and the phase ratio units are $\mathrm{mL\,mL^{-1}}$. The phase ratio represents therefore the ratio between the solid and the liquid phase volume:

$$\Phi_i = \frac{V_{S,i}}{V_{L,i}} = \frac{1-\varepsilon_i}{\varepsilon_i} \quad (3)$$

Actually, the retention is driven by the adsorption and partitioning of the solute on the alkyl layer on top of the stationary phase surface [10]. The amount adsorbed is therefore proportional to the surface accessible for adsorption and not to the solid phase volume accessible [11]. By normalizing the amount of component i adsorbed by the surface accessible for adsorption, one obtains a meaningful quantity that can be used to quantify and compare adsorption equilibria on different materials. In this case, the units of q_i become $\mathrm{mg\,m^{-2}}$ and the units of the phase ratio become $\mathrm{m^2\,mL^{-1}}$. The phase ratio represents therefore the ratio between the surface available for adsorption and the liquid phase volume:

$$\Phi_i = \frac{S_{acc,i}}{\varepsilon_i \cdot V_c} \quad (4)$$

In this manuscript, the former approach will be named the volume-specific approach and the latter one will be named the surface-specific approach. It is important to mention that all the equations introduced in this manuscript are valid for both approaches. However, the units of the different parameters might differ between the two approaches.

2.2. Retention in diluted conditions

By assuming infinitely fast mass transfer and negligible axial dispersion, Eq. (1) can be simplified into the mass balance of the ideal model of chromatography:

$$\left(1 + \Phi_i \frac{\partial q_{eq,i}}{\partial c_i}\right) \frac{\partial c_i}{\partial t} + u_{lin} \frac{\partial c_i}{\partial z} = 0 \quad (5)$$

The retention time for a certain concentration can be found by solving the previous differential equation with the method of characteristics [12]:

$$t_{R,i}(c_i) = t_{0,i}\left(1 + \Phi_i \left.\frac{\partial q_{eq,i}}{\partial c_i}\right|_{c_i}\right) \quad (6)$$

If $c \approx 0$, the initial slope of the adsorption isotherm (i.e. Henry coefficient) can be obtained from the measured retention time:

$$t_{R,i}(c) = t_{0,i}(1 + \Phi_i H_i) \quad (7)$$

The latter is related to the retention factor, k'_i, by the following equation:

$$k'_i = \Phi_i H_i \quad (8)$$

Note that the Henry coefficient obtained from Eq. (7) will be volume-specific if the volume-specific phase ratio is used and it will be surface-specific if the surface-specific phase ratio is used.

2.3. Mass transfer limitation

Using the results of Lapidus and Amundson [13], Van Deemter et al. have obtained the solution of Eq. (1) for an impulse injection assuming a Gaussian concentration profile [14]. This result was then used to define the height equivalent to a theoretical plate:

$$\mathrm{HETP}_i = \frac{2D_{L,i}}{u_{lin}} + 2\left(\frac{k'_i}{1+k'_i}\right)^2 \frac{u_{lin}}{k'_i k_{M,i}} \quad (9)$$

The axial dispersion coefficient, $D_{L,i}$, is given by:

$$D_{L,i} = \gamma D_{M,i} + \frac{\lambda u_{lin} \varepsilon_i d_P}{\varepsilon_b} = \gamma D_{M,i} + K_{eddy,i} \cdot u_{lin} \quad (10)$$

where $D_{M,i}$ is the molecular diffusion coefficient, K_{eddy} is the eddy diffusion parameter, d_p is the particle size, ε_b is the bed porosity and γ and λ are empirical parameters. The first term in Eq. (10) is related to the molecular diffusion and the second term to the eddy diffusion. The eddy diffusion parameter $K_{eddy,i}$ is related to the eddy diffusion coefficient, $D_{eddy,i}$ as follows:

$$D_{eddy,i} = K_{eddy,i} \cdot u_{lin} \quad (11)$$

It is important to note that $K_{eddy,i}$ is not a function of the mobile phase flow rate, whereas $D_{eddy,i}$ increases with the flow rate. In liquid chromatography, the mobile phase flow rate is relatively high and the molecular diffusion is in general negligible (i.e. the first term in Eq. (10)). In fact, considering that the molecular diffusion of a peptide in water–acetonitrile is in the order of 10^{-6} $\mathrm{cm^2/s}$, the first term in Eq. (10) is approximately equal to 7×10^{-7} $\mathrm{cm^2/s}$. The stationary phases used in this work have a particle diameter of 10 μm and the linear velocity is always larger than 0.035 cm/s. The second term in Eq. (10) is, therefore, ranging from 3×10^{-5} $\mathrm{cm^2/s}$ to 2×10^{-4} $\mathrm{cm^2/s}$ and it is dominant over the first one.

By neglecting the first term in Eq. (10) and by inserting the latter in Eq. (9), the following equation is obtained:

$$HETP_i = 2K_{eddy} + 2\left(\frac{k'_i}{1+k'_i}\right)^2 \frac{u_{lin}}{k'_i k_M} \quad (12)$$

2.4. Pore size distribution

The pore size distribution (PSD) of chromatographic stationary phases has been studied by several authors [15–19]. The most important techniques used to characterize the pore size geometry are inverse size exclusion chromatography, nitrogen adsorption and mercury porosimetry. In this paper, the PSD has been characterized by inverse size exclusion chromatography (iSEC), because

Table 1
Name and properties of the stationary phase materials used in this study.

Material	Particle size [μm]	pore volume [cm^3/g]	Surface area [m^2/g]	Pore size [Å]	carbon content [%]	C18 density [$\mu mol/m^2$]
Zeo100	10.7	0.37	216	89	17.5	2.5
Zeo120	10.7	0.41	159	133	16.9	3.5
Zeo150	10.7	0.42	156	138	16	3.2
Zeo200	10.7	0.47	120	199	11.9	3.4
Kova120	9.8	0.43	193	112	18.95	2.8
Kova200	9.4	0.63	139	231	12.6	3.4
Kova300	9.3	0.69	109	320	9.7	3.5

it is the most suitable technique to investigate the stationary phase structure in conditions similar to the chromatographic conditions (i.e. in a packed column).

In iSEC, a set of standard polymer probes with defined molecular mass and size are used to investigate the intra and extra particle volume. The retention volume of each molecule *i*, $V_{R,i}$, is measured under non-adsorbing conditions and the partition coefficient, $K_{SEC,i}$ is calculated:

$$K_{SEC,i} = \frac{V_{p,acc,i}}{V_{p,total}} = \frac{V_{R,i} - V_b}{V_{L,tot} - V_b} \tag{13}$$

where $V_{p,acc,i}$ is the pore volume accessible for molecule *i*, $V_{p,total}$ is the total pore volume, $V_{L,tot}$ is the total liquid volume of the column and V_b is the volume of the interparticle void volume. $K_{SEC,i}$ represents the fraction of pore volume accessible for a molecule *i*.

In reversed phase chromatography, injection of polystyrene standard in pure dichloromethane is the method of choice for the determination of the PSD [15–17]. In those conditions, the radius of the polystyrene standard, R_i, can be related to its molecular weight, MW_i, as follows [20]:

$$R_i = 0.621(MW_i)^{0.588} \tag{14}$$

The pore size distribution of chromatographic stationary phases can be typically represented with the log-normal distribution [4,18,19]:

$$f(r) = \frac{1}{r}\exp\left[-\frac{1}{2}\left(\frac{\log(r/r_p)}{s_p}\right)^2\right] \tag{15}$$

where $f(r)dr$ represents the pore volume that has a cross-sectional dimension in the range between r and $r+dr$. The parameters r_p and s_p provide a measure of the average value and width of the distribution, respectively.

In order now to relate the pore size distribution (Eq. (15)) to the pore accessibility we need to introduce some assumption about the pore geometry. Typically the pores are assumed to be cylindrical and the probe to be spherical. However, other shapes have also been considered [21]. In reality, the pores are much more irregular and the geometry assumption used in iSEC cannot really describe the actual pore heterogeneity. As a consequence, the iSEC results cannot be considered in absolute terms, but they can be used to compare different materials [19]. By modeling a spherical probe in a cylindrical pore, it is possible to correlate the partitioning coefficient of a compound of radius $r_{m,i}$ with the pore size distribution:

$$K_{SEC,i}(r_{m,i}) = \frac{V_{p,acc,i}}{V_{p,total}} = \frac{\int_{r_{m,i}}^{\infty} f(r)(1-(r_{m,i}/r))^2\,dr}{\int_{r_{\min}}^{\infty} f(r)(1-(r_{\min}/r))^2\,dr} \tag{16}$$

where $r_{\min}$ is the molecular radius of the smallest probe and therefore of the smallest pores considered. Similarly the accessible surface area for a molecule *i*, $A_{acc,i}$, can be calculated by the following equation:

$$A_{acc,i}(r_{m,i}) = \frac{\int_{r_{m,i}}^{\infty} 2/r(1-(r_{m,i}/r))f(r)\,dr}{\int_{r_{\min}}^{\infty} f(r)(1-(r_{\min}/r))^2\,dr} \tag{17}$$

Table 2
Composition of the buffers used in this study.

Experiment	Buffer	Composition
Synthetic peptide purification	A1	TFA/H_2O/AcN, 0.1/97.9/2 (v/v/v)
	B1	TFA/H_2O/AcN, 0.1/49.9/50 (v/v/v)
Synthetic peptide analytics	A2	Triethylamine phosphate, pH 2.25
	B2	A2/ Acetonitrile, 40/60 (v/v)
Insulin purification	A3	50 mM ammoniumacetate in 3.8% EtOH at pH 4
	B3	50 mM ammoniumacetate in 50% EtOH at pH 4
Insulin analytics	A4	50 mM ammoniumacetate in 25.3% EtOH at pH 4
	B4	50 mM ammoniumacetate in 38% EtOH at pH 4
Tanaka test	T1	MeOH/H_2O, 80:20 (v/v)
	T2	MeOH/H_2O, 25.3:74.7 (v/v)
	T3	MeOH/20 mM phosphate buffer at pH 2.7, 30:70 (v/v)
	T4	MeOH/20 mM phosphate buffer at pH 7.6, 30:70 (v/v)

3. Experimental

3.1. Chemicals

HPLC grade acetonitrile, phenol, benzylamine, butylbenzene, amylbenzene, o-terphenyl, triphenylene and the polystyrene standard set were purchased from Sigma–Aldrich (Buchs, Switzerland). HPLC grade ethanol was purchased from Scharlab (Barcelona, Spain). HPLC grade methanol, orthophosphoric acid 85%, ammonium acetate and ammonia solution 25% were purchased from Merck (Darmstadt, Germany). Tri-fluoroacetic acid was purchased from ACROS (Geel, Belgium). Caffeine was purchased from Alfa Aesar (Karlsruhe, Germany). HPLC grade dichloromethane was purchased from VWR (Leuven, Belgium) All the chemicals were used without further purification. The deionized water was purified with a Simpak2 unit (Millipore, MA, USA) before use.

The two peptides used in this work are a synthetic polypeptide crude mixture and a mixture of insulin and desmido-insulin peptide. Insulin was purchased from Sigma–Aldrich (Buchs, Switzerland). It was boiled in 0.01 M HCl at 40 °C for 1 day to obtain about 5% of desamido-insulin in the mixture. The synthetic polypeptide crude mixture is a 1.2 kDa polypeptide and is representative of an actual industrial product. It was kindly donated by Genzyme pharmaceuticals (Liestal, Switzerland).

3.2. Experimental setup and stationary phases

The experiments were carried out on an Agilent 1100 Series HPLC, equipped with an auto-sampler, a diode array detector, an online-degasser and a quaternary gradient pump. A Gilson FC 203B fraction collector (Middleton, WI, USA) was connected at the outlet of the HPLC to collect fractions during the peptide elution.

The stationary phases used in the study were provided by Zeochem AG (Uetikon, Switzerland). They are listed in Table 1. The materials were produced starting with two different bare silicas (Zeo and Kova). The same derivatization was applied to all materials using a monofunctional C18-silane followed by an end-capping with a small silane. The packed columns have 25 cm length and 0.46 cm internal diameter. The particle size was measured by laser diffraction using a Malvern Mastersizer S long bed equipped with dry powder feeder. The carbon content was obtained from elemental analysis using a TruSpec CHN from LECO. The pore volume and the BET surface area were measured by nitrogen adsorption on the functionalized material using a Micromeretics TriStar. The BET surface area values were corrected to account for the different area occupied by a nitrogen molecule on a hydrophobic surface ($S_{real} = S_{measured} \cdot (20.6/16.2)$) [6]. The pore volume was obtained from the desorption part of the nitrogen adsorption isotherm using the BJH technique [22]. The pore size was calculated from the BET surface area and the BJH pore volume assuming a cylindrical pore geometry.

The Kromasil 100 A 5 μm C18 4.6 mm × 250 mm was obtained from EKA chemicals AB (Bohus, Sweden). It was used to analyze the purity of the peptide fractions collected during the chromatographic experiments. The ZORBAX 300SB-C18 4.6 mm × 150 mm was obtained from Agilent Technologies (Santa Clara, United States). It was used to analyze the purity of the insulin fractions collected during the chromatographic experiments.

3.3. Buffer and analytics

The buffers used in this work have the compositions listed in Table 2. To analyze synthetic peptide fractions collected during overloaded experiments, a gradient from 34% B2 to 64% B2 was carried out in 40 min on the Kromasil 100 A 5 μm C18 column at a temperature of 55 °C. The UV response at 215 nm was recorded and calibrated using samples of known peptide concentration.

To analyze insulin peptide fractions collected during overloaded experiments, a gradient from 33% B4 to 70% B4 was carried out in 30 min on the ZORBAX 300SB-C18 column at a temperature of 40 °C. The UV response at 280 nm was recorded and calibrated using samples of known insulin concentration.

3.4. Tanaka test

The buffers used for the Tanaka test are listed in Table 2. The amylbenzene–butylbenzene selectivity measurement gives an estimate of the hydrophobic selectivity. The measurement is performed in mobile phase T1. The triphenylene-o-terphenyl selectivity is a measurement of the steric selectivity. This test is also carried out in mobile phase T1. The caffeine–phenol selectivity measurement gives an estimate of the hydrogen bond capacity. It is performed in mobile phase T2. The benzylamine–phenol selectivity measurements at low and high pH are carried out in buffer T3 and T4, respectively. These measurements give an estimate of the amount and acidity of the silanol groups. More details about the Tanaka test can be found in [23,24].

4. Results

4.1. Pore size distribution

The retention volumes of polystyrene standard ranging from 100 to 2,000,000 g/mol were measured on all materials using pure dichloromethane as eluent. The flow rate used for the polymers having molecular weight ranging from 100 to 1,000,000 was 0.5 mL/min while for larger polymers it was 0.1 mL/min as suggested by Guan-Sajonz and Guiochon [16]. A typical result is shown in Fig. 1 for the material Kova120. It can be seen that the iSEC data exhibit the classical two different behaviors corresponding to the retention contribution of the internal pores (diamonds) and of the external void volume (triangles). The bed porosity, ε_b, also referred to as the external porosity, was obtained from the extrapolation of the external void volume branch of the iSEC plot to $MW^{1/3} = 0$ [3]. The total column porosity, ε_{total}, was measured by pycnometry using acetonitrile and dichloromethane. The results for the bed and total column porosity are listed in Table 3. For all examined materials, it is seen that the bed porosity values are ranging from 0.37 to 0.4. These values are similar to the bed porosity values obtained by Guan-Sajonz and Guiochon for commercially available silica-based reversed phase material [16]. On the other hand, the total column porosity tends to slightly increase with the pore size.

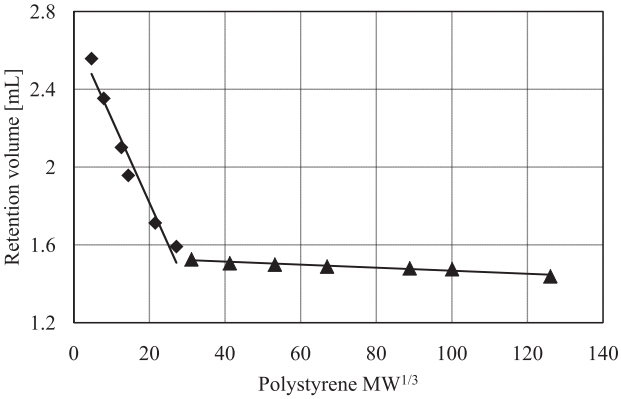

Fig. 1. Elution volume of polystyrene standard as a function of the cubic root of their molecular weight on the Kova120 material. Internal pore volume branch (diamonds), external void volume branch (triangles).

The partitioning coefficient for the different polystyrene standards was calculated using Eq. (13) and then fitted with Eqs. (15) and (16). The fitting was done in Matlab® using the fmincon function [25]. The obtained values of the fitting parameters, i.e. r_p and s_p, are reported in Table 3, while the comparison between experimental and calculated values is shown in Fig. 2 for all materials considered.

The porosity accessible for the two peptides considered in this work can be calculated using Eq. (16) together with the size evaluation for the two peptides provided by the correlation of Young et al. [26] and the stoke-Einstein equation as suggested by Gritti and Guiochon [4] (i.e. $R_{peptide} = 9.5$ Å and $R_{insulin} = 15.8$Å). The obtained values are compared in Table 3 with the corresponding experimental values measured in non-adsorbing conditions for all considered materials [27]. It can be seen that the experimental porosity is always lower than the calculated one. This underestimation of the porosity measured under non-adsorbing conditions is due to the electrostatic exclusion of the peptide from the pore and to the strong accumulation of modifier in the pore, which is preventing the peptide to access the entire porosity accessed by the neutral polystyrene standard in the absence of modifier (i.e. the pore size distribution was calibrated in pure dichloromethane) [27]. However, since these effects are also less prominent for the peptide under adsorbing conditions (i.e. lower modifier concentration), the calculated porosity obtained from iSEC measurements is more representative of the porosity accessible to the peptide in these conditions and therefore it has been used in the rest of this work.

Table 3
column properties, Eq. (18) fitting parameters and porosities accessible to the synthetic peptide and insulin for all materials in Table 1.

		Zeo100	Zeo120	Zeo150	Zeo200	Kova120	Kova200	Kova300
Material properties	ε_{total} [−]	0.61	0.62	0.62	0.64	0.61	0.69	0.71
	ε_b [−]	0.40	0.38	0.37	0.37	0.37	0.37	0.38
Eq. (18) fitting parameters	r_p [Å]	90.3	153.9	154.9	216.2	104.1	240.8	358.5
	s_p [−]	0.31	0.37	0.49	0.46	0.43	0.37	0.42
Porosity accessible to the peptide	$\varepsilon_{peptide,exp}$ [−]	0.47	0.53	0.51	0.55	0.44	0.59	0.64
	$\varepsilon_{peptide,calc}$ [−]	0.57	0.60	0.59	0.62	0.57	0.67	0.69
Porosity accessible to insulin	$\varepsilon_{insulin,exp}$ [−]	0.48	0.51	0.52	0.56	0.48	0.59	0.63
	$\varepsilon_{insulin,calc}$ [−]	0.55	0.58	0.57	0.61	0.54	0.65	0.68

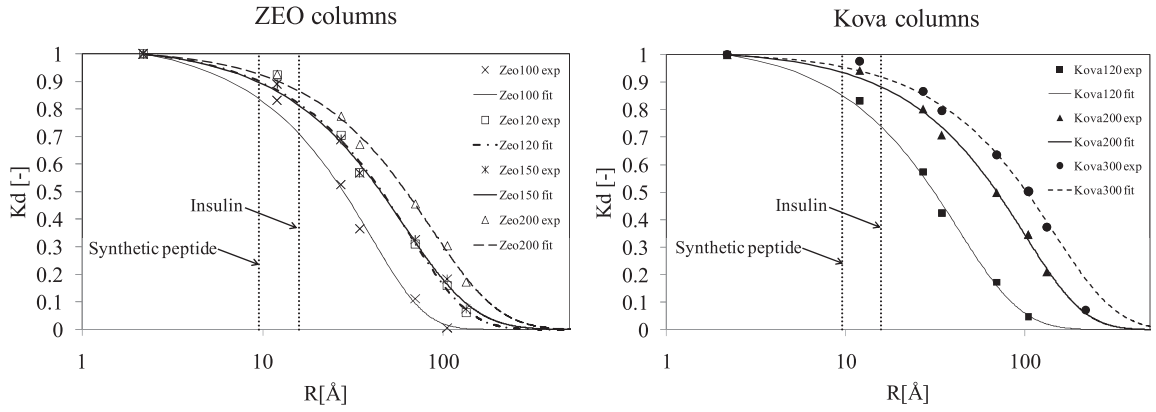

Fig. 2. Partition coefficient of polystyrene standard measured experimentally and fitted with Eq. (16) for the various materials in Table 1.

4.2. Van Deemter measurement

The HETP of the synthetic peptide and insulin were calculated from their retention time, t_R, and peak width at half height, $w_{1/2}$, in weakly adsorbing conditions ($k' \approx 3.2$) as follows:

$$\mathrm{NTP} = \frac{5.55 \cdot t_R^2}{w^2} \tag{18}$$

$$\mathrm{HETP} = \frac{L_c}{\mathrm{NTP}} \tag{19}$$

where NTP is the number of theoretical plate and L_c is the column length. The experimental HETP values were fitted with Eq. (12) and the obtained values of the eddy diffusion parameter, K_{eddy}, and mass transfer coefficient, k_m, are shown in Figs. 3 and 4, respectively. It can be seen that the eddy diffusion parameter of the peptides depend neither on the pore size nor on the peptide size. The differences observed between the columns are most likely due to packing inhomogeneities. On the other hand, the lumped mass transfer coefficient clearly increases with increasing pore size and decreasing peptide size. This is due to the fact that the pore diffusion is strongly dependent on the ratio between the molecule and the pore size [1].

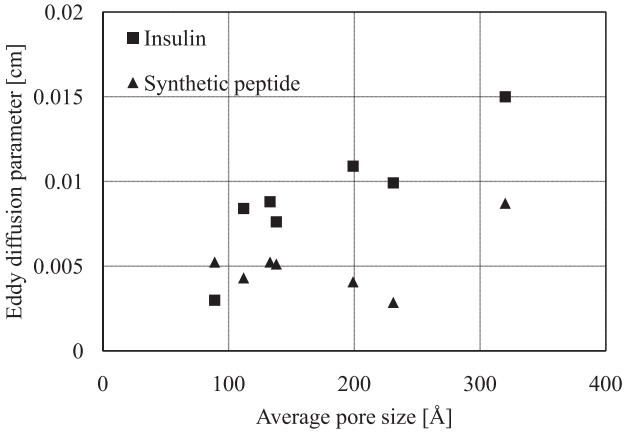

Fig. 3. Eddy diffusion parameter of the synthetic peptide and insulin as a function of the average pore size of the various materials in Table 1.

4.3. Adsorption in diluted conditions

The retention factor of the synthetic peptide and insulin has been measured on all columns and is shown in Fig. 5 as a function of the modifier concentration, i.e. acetonitrile and ethanol respectively. It can be seen that the retention factor of both peptides increases with decreasing pore size. This increase can be explained by an increase of the surface accessible for decreasing pore size. In order to quantify this explanation, the experimental retention factors have been plotted in Fig. 6 as a function of the surface specific phase ratio, Φ_i. It is found that a linear behavior is obtained in all cases and according to Eq. (8) the Henry coefficient is given for each modifier concentration by the slope of the corresponding straight line. The variation of the so obtained values of the surface-specific Henry coefficient with the modifier concentration is nicely fitted in Fig. 7 with the linear solvent strength theory:

$$\log(H_i) = \log(H_{w,i}) + m_i \varphi_{\mathrm{mod}} \tag{20}$$

where H_i is the Henry coefficient of component i, φ_{mod} is the volume fraction of the modifier and $H_{w,i}$ and m_i are fitting parameters.

4.4. Adsorption in overloaded conditions

Under overloaded conditions the adsorption isotherm of insulin and the synthetic peptide becomes non linear. Both gradient and isocratic overloaded chromatographic runs of the two peptides were performed and the measured elution profiles were fitted using the lumped kinetic model Eqs. (1) and (2) and a surface-specific

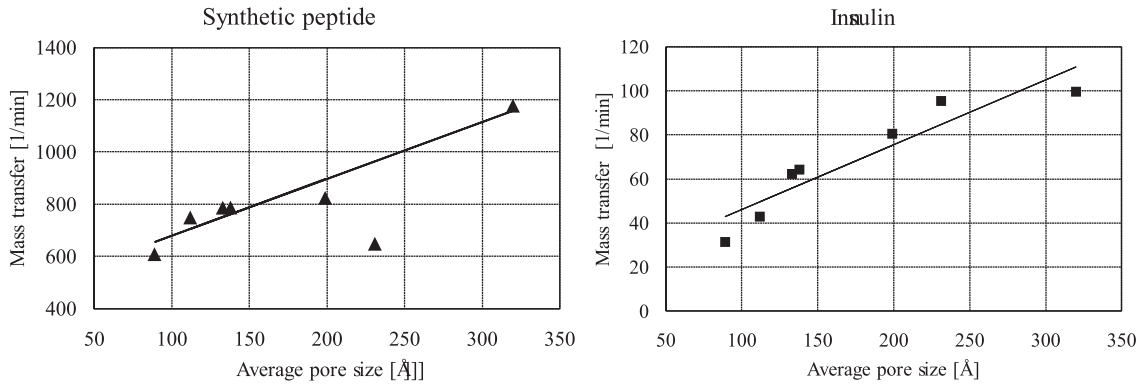

Fig. 4. Mass transfer coefficient of the synthetic peptide and insulin as a function of the average pore size of the various materials in Table 1.

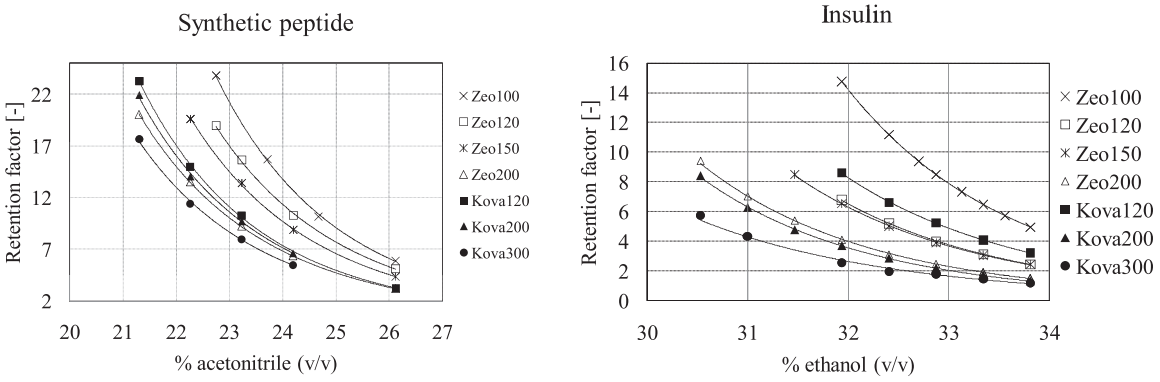

Fig. 5. Retention factor of the synthetic peptide and insulin as a function of the modifier concentration for all columns.

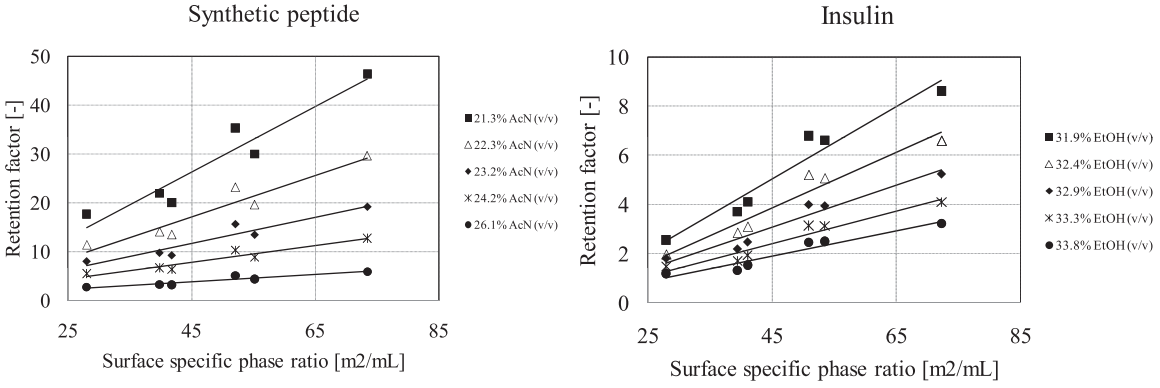

Fig. 6. Retention factor of the synthetic peptide and insulin as a function of the surface-specific phase ratio, $\Phi' i$, given by Eq. (4) for all columns. Straight lines represent the fitting with Eq. (8).

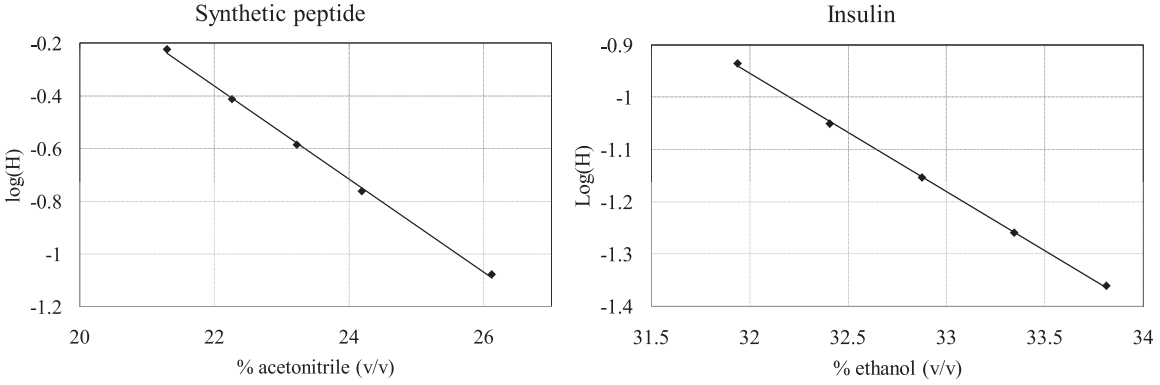

Fig. 7. Surface-specific Henry coefficient as a function of the modifier concentration. Straight lines represent fitting with Eq. (20). $\log(H_{w,\text{synthetic peptide}}) = 3.526$ and $m_{i,\text{synthetic peptide}} = -0.177$; $\log(H_{w,\text{insulin}}) = 6.291$ and $m_{i,\text{insulin}} = -0.2264$.

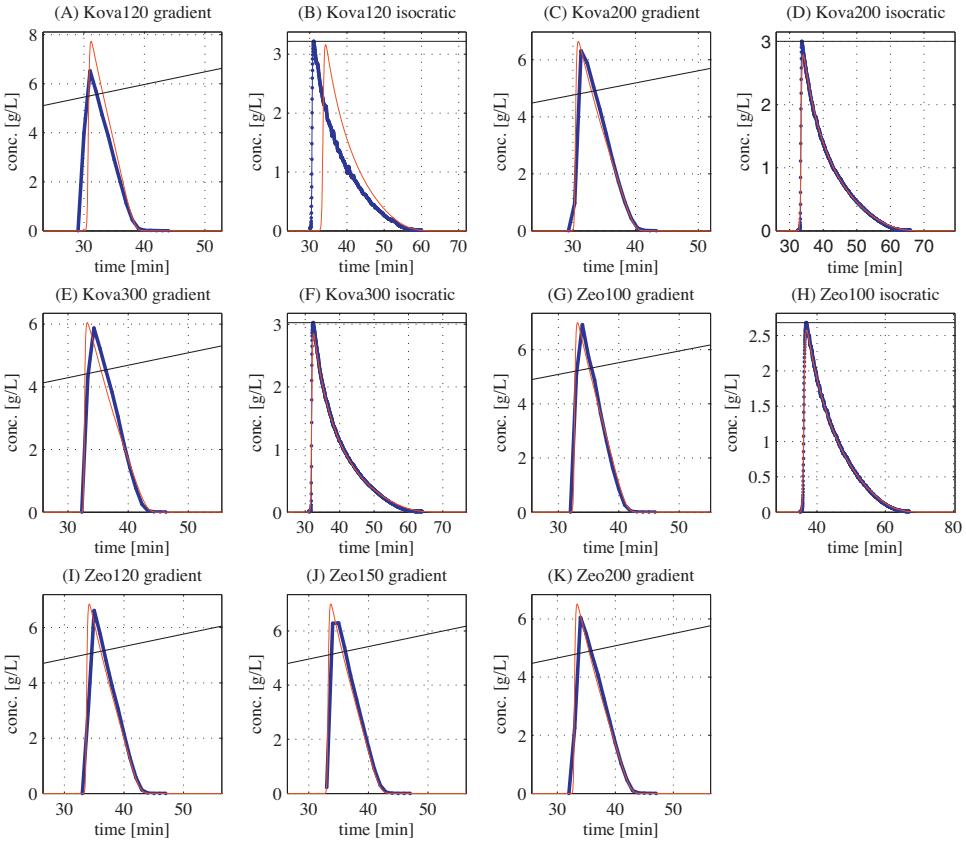

Fig. 8. Fitting of the experimental insulin overloaded elution profiles with the surface specific adsorption model.

bi-Langmuir isotherm:

$$q_{eq.i} = \frac{H_{1,i}c_i}{1+(H_{1,i}/q_{sat1,i})c_i} + \frac{H_{2,i}c_i}{1+(H_{2,i}/q_{sat2,i})c_i} \quad (21)$$

A bi-Langmuir isotherm was used to fit the elution profile in order to better reproduce the non-linearity of the elution profiles which could not be obtained using the Langmuir isotherm. In this model two specific adsorption sites are considered. Their corresponding Henry constants, $H_{1,i}$ and $H_{2,i}$ when added give the overall Henry constant value H_i estimated through Eq. (8), i.e. $H_{1,i} + H_{2,i} = H_i$. Moreover it was assumed that $H_{2,i}$ follows the linear solvent strength theory:

$$\log(H_{2,i}) = \log(H_{w2,i}) + m_{2,i}\varphi_{\text{mod}} \quad (22)$$

The saturation capacity of the two sites, $q_{sat1,i}$ and $q_{sat2,i}$, was allowed to vary with the Henry coefficient using the following saturation function:

$$q_{sat1,i} = \frac{\eta_{1,i}H_{1i}}{1+(\eta_{1,i}/q^0_{sat1,i})H_{1i}} \quad (23)$$

where $\eta_{1,i}$ is a parameter describing the rate of variation of the saturation capacity $q_{sat1,i}$ with the Henry coefficient of the first site, $H_{1,i}$ and $q^0_{sat1,i}$ is the maximum saturation capacity experienced when the modifier concentration is very low and therefore the Henry coefficient becomes very large. This is an empirical model that we have to introduce to describe gradient experiments since no theoretical model exists to describe the effect of the modifier concentration on the saturation capacity. The fitting of Eq. (21) to the overloaded elution profile was done in Matlab using the Lester Ingber's Adaptive Simulated Annealing gateway function [28]. The experimental conditions of the overloaded experiments used for the fitting are summarized in Table 4. The corresponding experimental elution profiles are shown in Figs. 8 and 9 while the estimated values of the fitting parameters, $H_{w2,i}$, $m_{2,i}$, $q^0_{sat1,i}$, $q^0_{sat2,i}$, $\eta_{1,i}$ and $\eta_{2,i}$ are listed in Table 5. It can be seen that the model is in

Table 4
Experimental conditions used in the overloaded experiments.

		Zeo100	Zeo120	Zeo150	Zeo200	Kova120	Kova200	Kova300
Synthetic peptide isocratic experiment	Loading [g/L column]	2	2	2	2	2	2	2
	Acetonitrile concentration [%B3]	46	44	44	43	43	43	42
Insulin isocratic experiment	Loading [g/L column]	6	-	-	-	6	6	6
	Ethanol concentration [%B3]	60	-	-	-	58	56	55
Synthetic peptide gradient experiment	Loading [g/L column]	4.34	4.34	4.34	4.34	4.34	4.34	4.34
	Starting gradient concentration [%B1]	20	18.2	18.5	17.1	20.2	16.9	15.1
	Gradient slope [%B1·min^{-1}]	0.5	0.5	0.5	0.5	0.5	0.5	0.5
Insulin gradient experiment	Loading [g/L column]	7.6	7.6	7.6	7.6	7.6	7.6	7.6
	Starting gradient concentration [%B3]	44.5	43.2	43.4	42.3	44.6	42.2	40.7
	Gradient slope [%B3·min^{-1}]	0.59	0.59	0.59	0.59	0.59	0.59	0.59

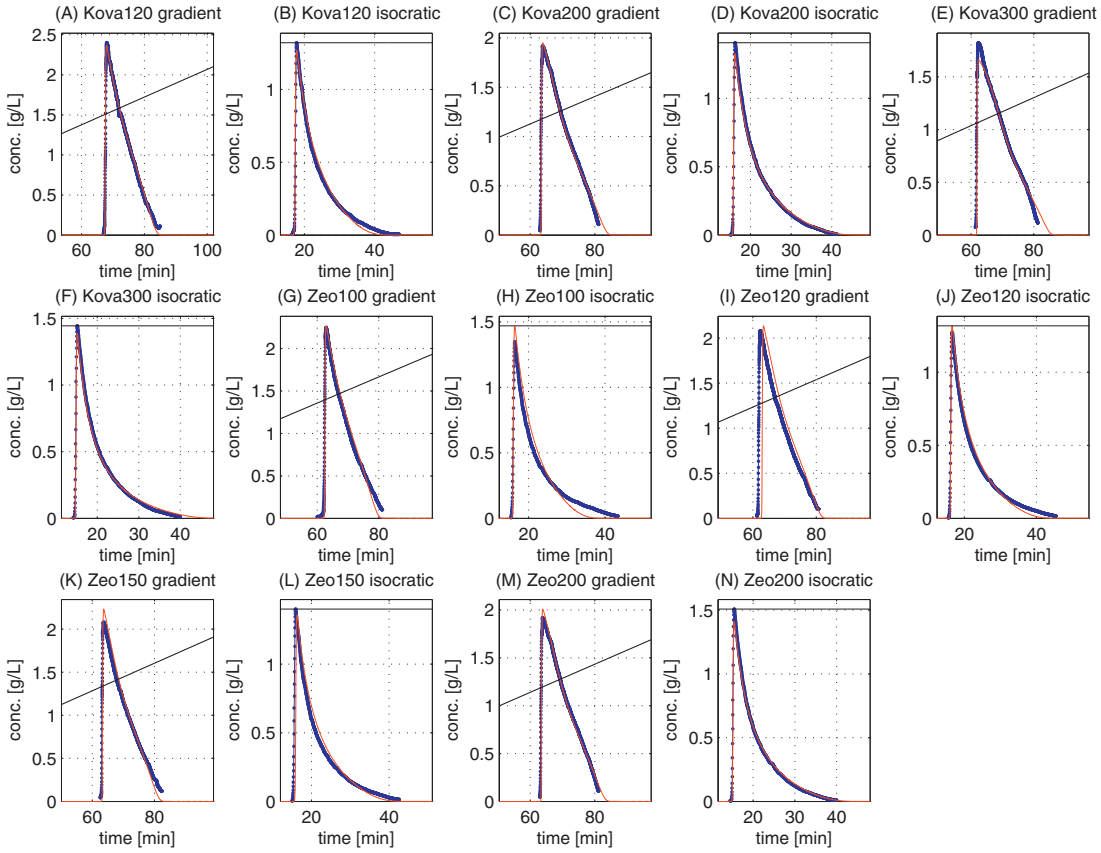

Fig. 9. Fitting of the experimental synthetic peptide overloaded elution profile with the surface-specific adsorption model.

very good agreement with the experimental elution profiles, except for the insulin elution on the Kova120. The reason for the slight mismatch observed in this case is not known. It is worth to mention at this point that it is also possible to use a volume-specific bi-Langmuir adsorption isotherm to model the elution profile of the two peptides. However, the volume-specific adsorption isotherm requires a complete set of isotherm parameters for each stationary phase. In this section, the elution profiles of both peptides were successfully modeled on all columns with only one set of adsorption parameters, by using a surface-specific adsorption isotherm (i.e. a total of 6 isotherm parameters were used per peptide). With this model, it is possible to predict the elution profile of the peptides on any stationary phase knowing its surface-specific phase ratio, as long as their chemical composition does not change.

4.5. Performance in purification processes

As mentioned above, two purification problems were used to investigate the effect of the pore size on the separation performance in overloaded conditions: the purification of a synthetic peptide from its crude mixture and the separation of insulin from desamido-insulin. In order to make a fair comparison between the different materials, the organic modifier gradients used for the peptide purifications were adjusted in order to have the same retention on each column. This was achieved by keeping the same gradient slope and by adjusting the modifier initial concentration. The detailed experimental conditions are summarized in the last two rows of Table 4.

Table 5
Parameters of the bi-Langmuir adsorption isotherm obtained by peak fitting.

Parameter	Synthetic peptide	Insulin
$\log(H_{w,2})$ [−]	2.889	3.534
m_2 [−]	−0.176	−0.136
η_1 [mg/mL]	31.86	211.7
$q^0_{sat1,i}$ [mg/m^2]	0.113	1.496
η_2 [mg/mL]	91.98	136.5
$q^0_{sat2,i}$ [mg/m^2]	0.6135	0.4325

During the elution, fractions were collected and analyzed with the analytical methods discussed in Section 3.3. The yield of the purification process has been computed for each column for various fixed purity values. The results obtained are presented in Fig. 10. It can be seen that the yield of the insulin purification process is not affected by the stationary phase pore size. However, an increase of the synthetic peptide purification yield with the stationary phase pore size is found. The yield reaches a maximum at a pore size of about 200 Å and decrease slightly for larger pore sizes.

In order to better understand the differences in separation efficiency observed, the selectivity between insulin and desamido-insulin and the selectivity of the closely eluting impurities of the synthetic peptide were measured in diluted conditions. The results are shown in Figs. 11 and 12, respectively. In Fig. 11, it can be seen that the selectivity between insulin and desamido-insulin changes as a function of the modifier concentration (here represented in terms of surface-specific Henry coefficient of the main peptide) in the same way for all considered materials. That is the selectivity in diluted conditions is independent of the pore size. These results are consistent with the constant yield observed for the overloaded purification of insulin as a function of the pore size shown in Fig. 10.

In the case of the synthetic peptide, it can be seen in Fig. 12 that, for the material Kova300, the early eluting impurity selectivity (i.e. impurities L1 and L2) is not affected by the adsorption strength (i.e. the surface-specific Henry coefficient). The average L1 and L2 selectivity was found to be 0.93 and 0.76 respectively. However,

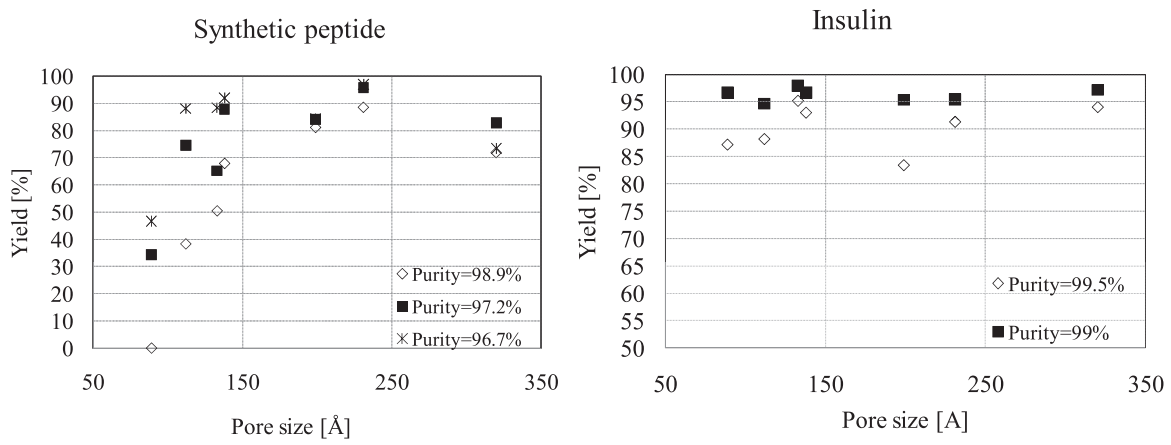

Fig. 10. Maximum yield obtained during the peptide purification process for various fixed purity values as a function of the stationary phase pore size.

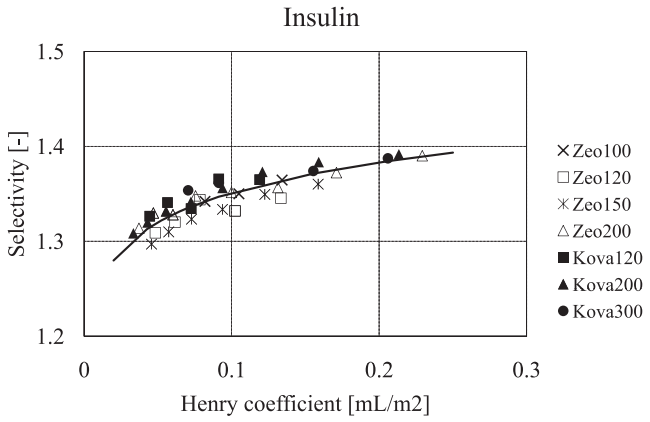

Fig. 11. Selectivity between insulin and desamido-insulin in diluted conditions.

the late eluting impurities selectivity (i.e. impurities S1 and S2) is a slight function of the surface-specific Henry coefficient. Similar results were obtained for all materials (not shown). The only significant difference refers to the selectivity of the impurity S1 which was found to significantly increase with the pore size as shown in Fig. 13. It is important to mention that the impurity S1 could not be seen on Zeo100, Zeo120 and Kova120 because it was almost co-eluting with the main peptide. Its selectivity on these materials was therefore extrapolated from the results obtained in Fig. 13.

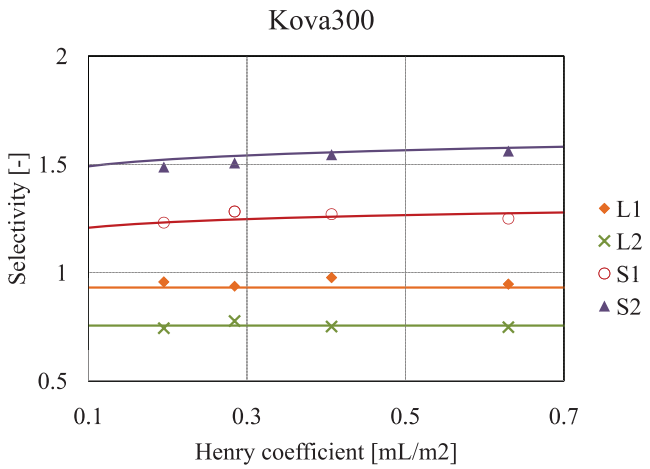

Fig. 12. Selectivity of the closest early (L1 and L2) and late (S1 and S2) eluting impurities of the synthetic peptide measured on Kova300.

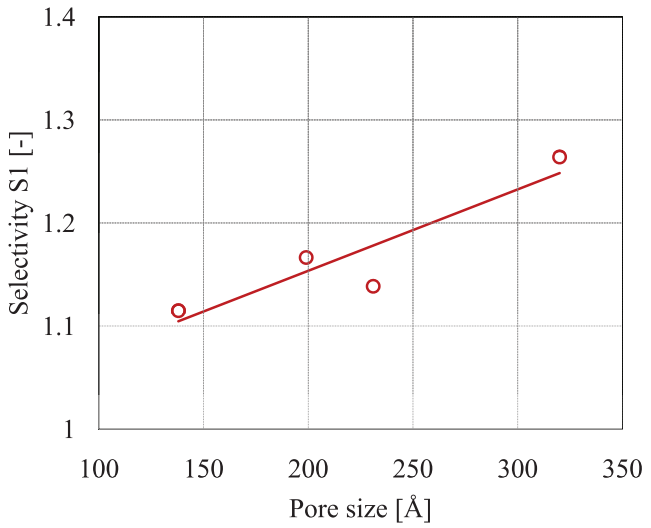

Fig. 13. Variation of the S1 impurity selectivity with the pore size measured at 21.9% acetonitrile (v/v).

This finding allows us to conclude that the change in the impurity S1 selectivity is the factor responsible for the change in the yield of the synthetic peptide purification process on the different materials. In fact, by comparing the overloaded elution profiles of

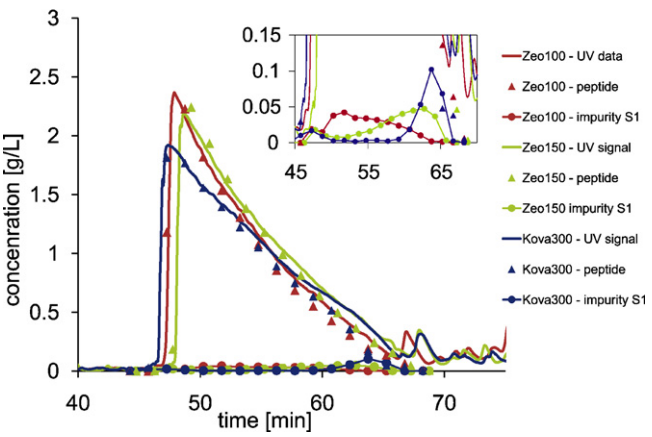

Fig. 14. Overloaded elution profiles of the synthetic peptide on the Zeo100, Zeo150 and Kova300. *Note*: impurity L1, L2 and S2 have been omitted to improve the clarity of the figure.

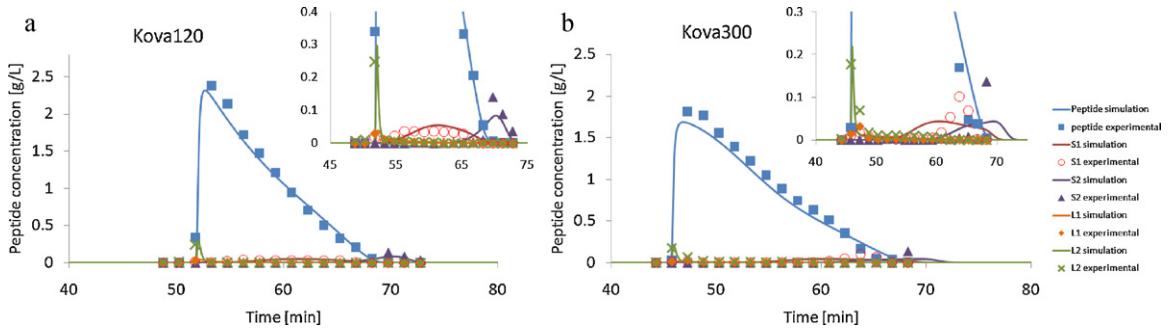

Fig. 15. Comparison of the experimental overloaded elution profile of the crude synthetic peptide (markers) with the model simulation (lines).

the crude synthetic peptide shown in Fig. 14, it can be seen that the decrease in impurity S1 selectivity exhibited by materials with decreasing pore size induces a displacement of the impurity below the main peak, which strongly affects the yield of the purification process.

In order to further prove this conclusion, the overloaded elution profiles of the synthetic peptide and the corresponding impurities were modeled using the lumped kinetic model (Eq. (1)) with a bi-Langmuir competitive adsorption isotherm:

$$q_{eq.i} = \frac{H_{1,i}c_i}{1+\sum_{j=1}^{n}(H_{1,j}/q_{sat1,j})c_j} + \frac{H_{2,i}c_i}{1+\sum_{j=1}^{n}(H_{2,j}/q_{sat2,j})c_j} \quad (24)$$

The values of the Henry coefficient and saturation capacity of the synthetic peptide were taken from Sections 4.3 and 4.4 respectively. For the impurities, the Henry coefficients were taken from their selectivity values while the saturation capacities were assumed to be equal to the main peptide saturation capacity [28]. The comparison between the experimental profile and the model, which have to be regarded as predictive since no parameter fitting has been made, is shown in Fig. 15. It can be seen that the experimental profile and the model predictions are in good agreement. Furthermore, the displacement of impurity S1 toward higher retention values with increasing pore size is confirmed by the model.

It can then be concluded that the change of the S1 impurity selectivity with the pore size is related to a variation of the affinity of the impurity toward the stationary phase surface (i.e. the Henry coefficient) and not to the change of mass transfer rate observed in Section 4.2. Such a change of selectivity must be due to a variation of the surface chemical characteristics.

4.6. Stationary phase surface properties

The Tanaka test was used to characterize the surface chemistry of the seven materials considered in this study [23]. The detailed experimental conditions can be found in Section 3.4. It was found that the amylbenzene–butylbenzene selectivity and the triphenylene-o-terphenyl selectivity do not change with the pore size, thus indicating a similar hydrophobic and steric selectivity for all materials. On the other hand, a decrease of the caffeine–phenol and benzylamine–phenol selectivity at both low and high pH was observed as shown in Fig. 16. Such a decrease indicates that the silanol activity decreases with increasing pore size. This observation is in agreement with the ligand density measurement. In fact, it can be seen in Fig. 17, that the ligand density tends to be lower in column having small pore sizes, thus leading to higher amount of unreacted silanol groups. The lower ligand density could be explained by a less efficient functionalization due to steric hindrance effect. The small variations of ligand density among the columns were however not sufficient to significantly affect the hydrophobicity of the column as the Tanaka test suggests.

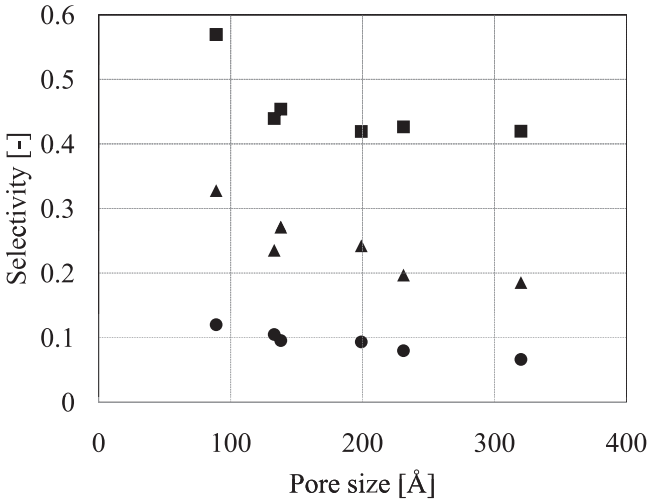

Fig. 16. Silanol activity of the various stationary phases as a function of the pore size. (square) caffeine–phenol selectivity. (triangles) benzylamine-phenol selectivity at high pH. (circles) benzylamine-phenol selectivity at low pH.

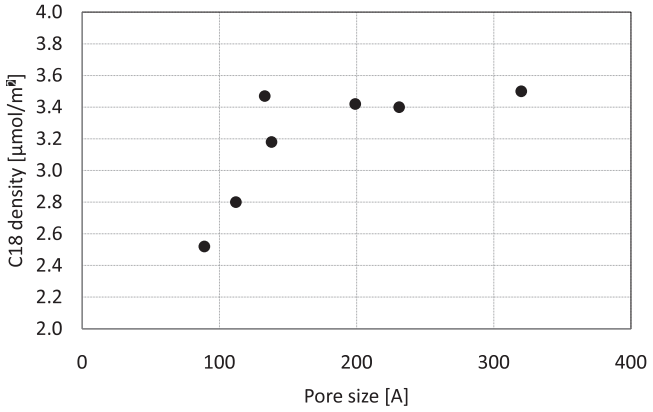

Fig. 17. Effect of the pore size on the ligand density.

It can therefore be concluded that the decrease in yield with increasing pore size observed for the synthetic peptide purification in the previous section is due to a decrease of the impurity S1 selectivity caused by an increase in silanol activity. A similar decrease of the impurity selectivity due to the silanol activity was already observed by Getaz et al. [24]. This change is not observed in the case of the insulin/desamido-insulin separation. This is not surprising since the effect of the silanol groups on selectivity is analyte specific [24].

5. Conclusions

The effect of the pore size of the stationary phase on the reversed phase chromatographic purification of two peptides (i.e. a synthetic peptide and insulin) has been investigated. As expected, it was found that the lumped mass transfer coefficient was linearly increasing with the pore size, leading to a decrease of the HETP with the pore size. However, it has been shown that this has no significant impact on the efficiency of the purification process of the two peptides.

The peptide retention in diluted conditions and the peptide elution profile in overloaded conditions were measured on various stationary phases with different pore sizes. The results were fitted with a surface-specific bi-Langmuir isotherm. This model takes into account the surface accessible for adsorption and allows using only one isotherm for all the materials with different pore sizes. The model was in good agreement with the experimental data.

The efficiency of the overloaded separation of insulin from desamido-insulin was evaluated for each material. It was found that the separation efficiency is not affected by the pore size. The results were in agreement with selectivity measurements performed in diluted conditions. On the other hand, in the case of the synthetic peptide, it was observed that the separation efficiency was in fact decreasing with decreasing pore size. This was explained by a decrease in selectivity of a closely eluting impurity with decreasing pore size. The selectivity decrease was attributed to a small increase of the silanol activity which has been confirmed experimentally using the Tanaka test. The change in separation efficiency with the pore size was confirmed through simulations with a lumped kinetic model including a surface-specific competitive adsorption isotherm.

From the results obtained in this work, it can be concluded that stationary phases with larger pore size are not enhancing the separation efficiency in preparative conditions for the two peptides investigated. This is because, in these conditions, the separation efficiency is not limited by mass transfer. On the other hand, the important factor to be considered for the preparative purification of peptides are the selectivity in diluted conditions and the competitive adsorption of the main peptide and the impurities in overloaded conditions, which we found to be strongly affected by the residual silanol activity at least for one of the two peptide considered.

Acknowledgments

The authors would like to gratefully acknowledge Dr. Gerhard Heizmann and Dr. Marc New from Genzyme Pharmaceuticals for their support.

References

[1] K. Yang, Y. Sun, Biochem. Eng. J. 37 (2007) 298.
[2] B.W. Sands, Y.S. Kim, J.L. Bass, J. Chromatgr. 360 (1986) 353.
[3] F. Gritti, A. Cavazzini, N. Marchetti, G. Guiochon, J. Chromatogr. A 1157 (2007) 289.
[4] F. Gritti, G. Guiochon, J. Chromatogr. A 1176 (2007) 107.
[5] Y.V. Kazakevich, J. Chromatogr. A 1126 (2006) 232.
[6] A. Giaquinto, Z. Liu, A. Bach, Y. Kazakevich, Anal. Chem. 80 (2008) 6358.
[7] A.V. Kiselev, J. Chromatogr. 49 (1970) 84.
[8] G. Foti, M.L. Belvito, A. Alvarez-Zepeda, E.sz. Kovats, J. Chromatogr. A 630 (1993) 1.
[9] G. Guiochon, A. Felinger, D.G. Shirazi, A.M. Katti, Fundamentals of Preparative and Nonlinear Chromatography, Academic Press, San Diego, CA, 2006.
[10] A. Vailaya, C. Horváth, J. Chromatogr. A 829 (1998) 1.
[11] R. Douglas, Principles of Adsorption and Adsorption Processes, John Wiley and Sons, 1984.
[12] H. Rhee, R. Aris, N.R. Amundson, First-order Partial Differential Equations, vol. 1, Dover Publications, 2001.
[13] L. Lapidus, N.R. Amundson, J. Phys. Chem. 56 (1952) 984.
[14] J.J. Van Deemter, F.J. Zuiderweg, A. Klinkenberg, Chem. Eng. Sci. 5 (1956) 271.
[15] I. Halász, K. Martin, Angew. Chem. Int. Ed. Engl. 17 (1978) 901.
[16] H. Guan-Sajonz, G. Guiochon, J. Chromatogr. A 731 (1996) 27.
[17] H. Guan-Sajonz, G. Guiochon, E. Davis, K. Gulakowski, D.W. Smith, J. Chromatogr. A 773 (1997) 33.
[18] Y. Yao, A.M. Lenhoff, J. Chromatogr. A 1037 (2004) 273.
[19] P. DePhillips, A.M. Lenhoff, J. Chromatogr. A 883 (2000) 39.
[20] M.E. Van Kreweld, N. Van den Hoed, J. Chromatogr. 83 (1973) 111.
[21] P. Dechadilok, W.M. Deen, Ind. Eng. Chem. Res. 45 (2006) 6953.
[22] E.P. Barrett, L.G. Joyner, P.P. Halenda, J. Am. Chem. Soc. 73 (1951) 3155.
[23] K. Kimata, K. Iwaguchi, S. Onishi, K. Jinno, R. Eksteen, K. Hosoya, M. Araki, N. Tanaka, J. Chromatogr. Sci. 27 (1989) 721.
[24] D. Getaz, M. Gencoglu, N. Forrer, M. Morbidelli, J. Chromatogr. A 1217 (2010) 3531.
[25] http://www.mathworks.com/help/toolbox/optim/ug/fmincon.html.
[26] M.E. Young, P.A. Carroad, R.L. Bell, Biotechnol. Bioeng. 22 (1980) 947.
[27] D. Getaz, G. Stroehlein, M. Morbidelli, J. Chromatogr. A 1216 (2009) 933.
[28] http://www.igi.tugraz.at/lehre/MLA/WS01/asamin.html.